De novo fabrication of custom-sequence plasmids for the synthesis of long DNA constructs with extrahelical features

Ramírez Montero, Daniel; Liu, Zhaowei; Dekker, Nynke H.

DOI
10.1016/j.bpj.2023.11.008

Publication date
2023

Document Version
Final published version

Published in
Biophysical journal

Biophysical Journal
Article

Biophysical Society

De novo fabrication of custom-sequence plasmids for the synthesis of long DNA constructs with extrahelical features

Daniel Ramírez Montero,[1] Zhaowei Liu,[1] and Nynke H. Dekker[1,*]
[1]Department of Bionanoscience, Kavli Institute of Nanoscience, Delft University of Technology, Delft, the Netherlands

ABSTRACT DNA constructs for single-molecule experiments often require specific sequences and/or extrahelical/noncanonical structures to study DNA-processing mechanisms. The precise introduction of such structures requires extensive control of the sequence of the initial DNA substrate. A commonly used substrate in the synthesis of DNA constructs is plasmid DNA. Nevertheless, the controlled introduction of specific sequences and extrahelical/noncanonical structures into plasmids often requires several rounds of cloning on pre-existing plasmids whose sequence one cannot fully control. Here, we describe a simple and efficient way to synthesize 10.1-kb plasmids de novo using synthetic gBlocks that provides full control of the sequence. Using these plasmids, we developed a 1.5-day protocol to assemble 10.1-kb linear DNA constructs with end and internal modifications. As a proof of principle, we synthesize two different DNA constructs with biotinylated ends and one or two internal 3′ single-stranded DNA flaps, characterize them using single-molecule force and fluorescence spectroscopy, and functionally validate them by showing that the eukaryotic replicative helicase Cdc45/Mcm2-7/GINS (CMG) binds the 3′ single-stranded DNA flap and translocates in the expected direction. We anticipate that our approach can be used to synthesize custom-sequence DNA constructs for a variety of force and fluorescence single-molecule spectroscopy experiments to interrogate DNA replication, DNA repair, and transcription.

SIGNIFICANCE Single-molecule studies of DNA-protein interactions often require DNA constructs containing specific sequence features. However, current methods to synthesize such DNA constructs lack full control of their sequence. We describe a way to assemble 10-kb plasmids from custom-sequence gBlocks, providing full control of their sequence. Using these plasmids, we developed a protocol to synthesize fully custom-sequence linear DNA constructs with biotinylated ends and internal 3′ flaps. Furthermore, we biophysically characterized these constructs and functionally validated them by showing that the eukaryotic replicative helicase binds the internal 3′ flap and translocates in the expected direction. We anticipate that our approach will help the single-molecule biophysics community to study the effect of DNA sequence on many important DNA-processing mechanisms with unprecedented control.

INTRODUCTION

Single-molecule studies of many DNA-processing mechanisms often require DNA constructs with specific sequence features important for the biological process being studied (e.g., origins of replication, promoter regions, and nucleosome-positioning sequences) (1–8). Furthermore, such studies may also require extrahelical and/or noncanonical structural features at defined positions within the DNA construct (1,9–15), the controlled incorporation of which often requires specific restriction sites at defined locations within the starting DNA substrate (1,11,14,16–20). Controlling the sequence of the starting DNA substrate used to synthesize DNA constructs for single-molecule studies is therefore of utmost importance.

Several essential DNA-processing mechanisms, such as DNA replication, transcription, and DNA compaction, are carried out by protein complexes evolved to cruise through thousands of base pairs (5,8,10,13,21–27). Therefore, to study such processes at a biologically relevant spatial scale, single-molecule experiments often require DNA constructs of several kilobases in length (4,5,8,11,13,14,18,21,23,24,27–30). In such long constructs, extrahelical and/or noncanonical DNA structures can be used as a specific binding site for the protein complex being studied (10–13) or to study the outcome of their encounter by the protein

Submitted August 28, 2023, and accepted for publication November 13, 2023.

*Correspondence: n.h.dekker@tudelft.nl

Editor: Jie Yan.
https://doi.org/10.1016/j.bpj.2023.11.008

complex after having established a baseline behavior of the complex on long stretches of duplex DNA (1,14,15).

A commonly used starting substrate to synthesize DNA constructs for single-molecule experiments given its length of ~48.5 kb and commercially availability is λ phage DNA (1,11,14,18,28,31–33). Nonetheless, engineering the sequence of the λ phage genome requires complex molecular cloning that is typically low in efficiency or requires the purification of specialized proteins (34–36). Furthermore, the incorporation of internal modifications into the λ phage genome can only be done in dispensable genomic regions (1,11). An alternative starting substrate to synthesize constructs for single-molecule studies is PCR-synthesized DNA, which, combined with oligonucleotide-based structures, has been used to successfully synthesize DNA constructs containing internal noncanonical/extrahelical structures such as hairpins (20), single-stranded DNA (ssDNA) flaps (37), and Holiday junctions (15). These PCR-based methods, however, either require multiple low-efficiency ligation steps, thus having low overall yields of the desired final product (20,37), or require the incorporation of abasic sites into the final construct (15), which can affect the behavior of DNA-binding proteins (38). An alternative starting substrate for single-molecule DNA constructs is plasmid DNA, which is commonly used given the ease with which large amounts of it can be generated by bacterial propagation (4,5,8,13,14,19,30,39–42). Although, using standard molecular cloning techniques, plasmids are easier to engineer than phage genomes, controlling the number and the position of restriction enzyme sites within the plasmid (which are required to introduce extrahelical modifications or noncanonical DNA structures) often involves several rounds of multi-day molecular cloning to either add desired restriction sites or to remove unwanted ones. Furthermore, commonly used plasmid substrates for single-molecule experiments are based on λ phage DNA (4,8,19,40–42), which can make cloning particularly difficult as these plasmids are typically very large in size and contain repetitive sequences. We currently lack a way to fully control the sequence of the initial plasmid DNA substrate used to synthesize DNA constructs for single-molecule studies, which is particularly important for the site-specific incorporation of extrahelical and/or noncanonical structures.

One type of extrahelical structure commonly incorporated into single-molecule constructs is ssDNA flaps, which can be used to load helicases and other proteins onto the DNA as it mimics a DNA unwinding intermediate (10,12,13,29,37). To date, ssDNA flaps are usually incorporated into DNA constructs in the form of pre-folded oligo-based Y-shaped structures ligated at the end of long (10–50 kb) DNA molecules (10,13,19,29). Nonetheless, in correlative optical tweezer and fluorescence single-molecule experiments (43), having the binding site for, e.g., a fluorescently labeled helicase at the end of the DNA is nonideal, as the end of the DNA is close to the trapping laser, which decreases the lifetime of fluorophores (44). Additionally, the end of the DNA is in direct contact with the protein-coated beads used for optical trapping experiments, which may 1) decrease the accessibility of the helicase binding site by steric hindrance and 2) result in nonspecific adhesion of the helicase to the beads. Previous PCR-based approaches have incorporated ssDNA flaps internally in shorter (~3.7 kb) DNA constructs via a time-consuming method involving several rounds of ligations (37). Alternatively, a nicking-based approach (16,17) has successfully introduced an internal ssDNA flap into λ phage genomic DNA (11). This approach, however, requires complex phage genome engineering, and the incorporation of extrahelical structures is limited to specific dispensable regions in the λ phage genome (11). We therefore lack a method to synthesize long (≥10 kb) linear DNA constructs for single-molecule studies with modified ends for surface attachment, as well as internal extrahelical and/or noncanonical structures, that 1) provides full control of the DNA sequence and 2) takes less than a couple of days to complete.

Here, we describe an effective way to assemble two different 10.1-kb plasmids de novo from synthetic fragments with fully custom-made sequences. This provides full control of the sequence without having to modify pre-existing plasmids; the de novo synthesis and validation of these plasmids takes 3–4 days. With this in hand, we develop a 1.5-day-long method that uses these custom-sequence plasmids to synthesize 10.1-kb linear DNA constructs with end and internal modifications, suitable for single-molecule experiments. As a proof of principle, we synthesize two linear 10.1-kb DNA constructs with three biotins at each end and with either one or two internal 3′ ssDNA flaps, and characterize them in bulk and with force and fluorescence single-molecule spectroscopy. Finally, we functionally validate our synthesized constructs at the single-molecule level by showing that the eukaryotic replicative helicase Cdc45/Mcm2-7/GINS (CMG) can specifically bind the internal 3′ ssDNA flap and then translocate in the expected 3′-to-5′ direction. Although we focus here on introducing 3′ flaps, our fully custom-sequence and versatile approach to the synthesis of DNA constructs for single-molecule studies can be easily generalized to constructs with several other extrahelical and/or noncanonical structures at desired sequences.

MATERIALS AND METHODS

Plasmid synthesis

gBlock design

All gBlocks used in this study were purchased from Integrated DNA Technologies (Table S1 in the Supporting Material). gBlocks were designed to contain overlapping sequences of 25–28 bp and a T_m of ~60°C–63°C at both ends for their assembly into custom-sequence plasmids. Notably, at least one of the gBlocks used to assemble a plasmid de novo must contain a bacterial origin of replication for bacterial propagation of the plasmid as well as an antibiotic resistance marker.

De novo assembly of pDRM1 and pDRM2 from custom-made gBlocks

pDRM1 and pDRM2 were assembled by incubating 0.016 pmol of gBlocks 1, 2, 3, and 4 (for pDRM1) or gBlocks 3, 5, 6, and 7 (for pDRM2) (Table S1) in 20 μL of 1× NEBuilder HiFi DNA Assembly Master Mix (NEB #E2621S) and incubated at 50°C for 120 min. The assembly reactions were then directly transformed into NEB 5-alpha Competent *E. coli* (High Efficiency) cells (NEB # 02987). Transformed cells were plated on Luria-Bertani medium (LB) agar plates supplemented with 50 μg/mL ampicillin and incubated at 37°C overnight. Individual clones were selected, grown overnight at 30°C in LB medium supplemented with 50 μg/mL ampicillin with 180 rpm shaking, and stored at −80°C in LB medium supplemented with 14% glycerol. A swab of the glycerol stocks was inoculated into 200 mL of LB medium supplemented with 50 μg/mL ampicillin and grown overnight at 30°C. Plasmids were then purified using a Macherey-Nagel NucleoBond Xtra Midi Plus (Bioké # 740412.50). The overlapping ends of the gBlocks used to assemble pDRM1 as well as key regions in pDRM1 were sequenced with oligos DRM_140, DRM_141, DRM_142, DRM_143, DRM_144, and DRM_145. The overlapping ends of the gBlocks used to assemble pDRM2 as well as key regions in pDRM2 were sequenced with oligos DRM_140, DRM_142, DRM_143, DRM_144, DRM_177, DRM_180, DRM_181, and DRM_182 (Table S2 in the Supporting Material). Plasmid maps of pDRM1 (Data S1) and pDRM2 (Data S2) can be found in the Supporting Material.

Test digestions of pDRM1 and pDRM2

Here, 400 ng of either pDRM1 or pDRM2 were digested for 2 h at 37°C in a final volume of 25 μL of 1× CutSmart buffer (NEB #B7204) with 0.8 μL of one, two, or three of the following enzymes: XhoI (NEB #R0146S), BsaI-HFv2 (NEB #R3733L), BbvCI (NEB #R0601S), Nb.BbvCI (NEB #R0631L), and AscI (NEB #R0558S). The reaction mixtures were then incubated at 80°C for 20 min to inactivate the restriction enzymes and then run on a 0.8% agarose gel stained with ethidium bromide.

Synthesis of pZL7

pDRM1 was linearized by PCR using primers Vector.FOR and Vector.REV, and a 393-bp fragment was inserted using NEBuilder HiFi DNA Assembly Master Mix (NEB #E2621S) to generate plasmid pER1. Then, NdeI, AscI, and NcoI restriction enzyme sites were inserted into pER1 by amplifying the plasmid by PCR using primers ZL3 and ZL4, followed by PCR amplification of the resulting plasmid using primers ZL7 and ZL8, and PCR amplification of the resulting plasmid using primers ZL13 and ZL14, to generate plasmid pZL1. A 3.1-kb fragment of pZL1 was duplicated twice into the same plasmid using a previously reported protocol (45). Briefly, pZL1 was digested with NcoI-HF (NEB #R3193S) to construct the plasmid backbone for fragment insertion. Then, a 3.1-kb insert was generated by the digestion of pZL1with NdeI (NEB #R0111S) and AscI (NEB #R0558S). The plasmid backbone was mixed with 1.2-fold molar excess of the 3.1-kb insert in 1× NEBuilder HiFi DNA Assembly Master Mix (NEB #E2621S). The reaction mixture was incubated at 50°C for 15 min, and subsequently transformed into NEB 5-alpha Competent *E. coli* (High Efficiency) cells (NEB # 02987) to propagate the assembled plasmid product, named pZL3. The aforementioned digestion and insertion protocol was repeated using pZL3 as the plasmid backbone and the 3.1-kb fragment from pZL1 to generate pZL7. A plasmid map of pZL7 (Data S3) can be found in the Supporting Material.

Synthesis of single-molecule constructs from pDRM1 and pDRM2

Plasmid linearization

Here, 10 μg of either pDRM1, pDRM2, or pZL5 were linearized overnight with 50 units of XhoI (NEB #R0146S) in 1× CutSmart buffer (NEB #B7204) in a final volume of 50 μL. The reaction mixture was then incubated at 65°C for 20 min to inactivate XhoI.

Biotinylation of DNA ends

Here, 50-μL XhoI linearization reactions were supplemented with 33 μM dGTP (Invitrogen # 10218014), 33 μM Biotin-14-dATP (Invitrogen # 19524-016), 33 μM Biotin-14-dCTP (Invitrogen # 19518-018), 33 μM Biotin-16-dUTP (Jena Bioscience # NU-803-BIO16), 15 units of Klenow fragment (3'→5' exo-) (NEB #M0212L), 4 μL of 10× NEBuffer 2 (NEB #B7002S), and water to a final volume of 90 μL and incubated at 37°C for 30 min. EDTA was then added at a final concentration of 10 mM to terminate the reaction, and the reaction mixture was incubated at 75°C for 20 min to inactivate the Klenow fragment. Unincorporated nucleotides were removed with a Microspin S-400 HR spin column equilibrated in Tris/EDTA (TE) buffer (GE Healthcare # GE27-5140-01) as follows: columns were vortexed and centrifuged for 1 min at 0.8 g, then 100 μL of biotinylation reaction was loaded onto the packed resin, centrifuged for an additional 2 min at 0.8 g, and the flowthrough collected in a new tube.

Nicking of biotinylated DNA

Biotinylated DNA (∼90 μL) was supplemented with 11 μL of 10× CutSmart buffer (NEB #B7204), 50 units of nicking enzyme Nb.BbvCI (NEB #R0631L), and water to a final volume of 110 μL and incubated at 37°C for 5 h. The reaction mixture was then incubated at 80°C for 20 min to inactivate Nb.BbvCI.

Fluorescent flap oligo annealing

Flap oligo DRM_186 (for construct C-DRM1), or DRM_159 (for construct C-DRM2), or ZL_15 (for construct C-ZL7) was added in 100-fold molar excess to the nicked DNA. The mixture was then heated to 80°C for 10 min and cooled down to 20°C at a rate of −1°C/min in a thermocycler.

Ligation and purification

The annealed oligo was ligated overnight at 16°C in 1× CutSmart buffer (NEB #B7204) supplemented with 1.5 mM ATP (Thermo Scientific #R0441) and 1600 units of T4 DNA ligase (NEB #M0202L) in a final volume of 120 μL. The ligation reaction was then run on a 0.8% agarose gel pre-stained with SYBR Safe (Invitrogen #S33102) and the final product band was excised and purified using Promega's Wizard SV Gel and PCR Clean-Up System (Promega # A9282).

Oligo labeling efficiency measurements

Labeling efficiencies of flap oligos DRM_186 and DRM_159 were measured to be 103% ± 5% and 105% ± 5%, respectively, by measuring the absorption at 550 nm.

Protein purification and labeling

$CMG^{Cdc45\text{-}S6}$ purification

ySMG14 S6-iFLAG-CDC45 CBP-MCM3 strain was a gift from the laboratory of John Diffley (Francis Crick Institute, UK). CMG was then expressed and purified as previously reported (24).

$CMG^{Cdc45\text{-}S6}$ labeling

$CMG^{Cdc45\text{-}S6}$ protein was fluorescently labeled by adding equimolar Sfp transferase and 4.5-fold molar excess of LD555-CoA fluorophore. The reaction mixture was incubated at 25°C for 1 h followed by purification using a Superose 6 3.2/300 column (Cytiva) equilibrated in CMG buffer (25 mM HEPES-KOH pH 7.6, 2 mM magnesium acetate, 0.02% Tween-20, 100 mM NaCl, and 10% glycerol).

Single-molecule imaging and force spectroscopy

Single-molecule fluorescence imaging and force spectroscopy

Single-molecule experiments were conducted on an instrument that combines optical tweezers and confocal microscopy (C-Trap, LUMICKS). This instrument is equipped with a microfluidic flow cell with four inlets and one outlet. Three of these channels are injected from the left and used for bead trapping, DNA/DNA:protein complex trapping and imaging, respectively. The other channel is used as a buffer exchange location. Before each experiment, the microfluidic flow cell and the tubing of the instrument were passivated for at least 30 min with 1 mg/mL bovine serum albumin (BSA, NEB #B9000S) followed by 0.5% Pluronic F-127 (Sigma #P2443).

The channels contained the following solutions:

Channel 1: 1.76-μm-diameter streptavidin-coated polystyrene beads (Spherotech) diluted 1:1000 in PBS.

Channel 2: 5 pM DNA in PBS (in the cases of C-DRM1 and C-DRM2) or 10 pM DNA prebound by CMG in CMG imaging buffer (250 mM potassium glutamate, 25 mM HEPES-KOH pH 7.6, 10 mM magnesium acetate, 0.02% NP40, 1 mM DTT, 0.1 mg/mL BSA, 2 mM 1,3,5,7 cyclooctatetraene, 2 mM 4-nitrobenzyl alcohol, 2 mM Trolox, 0.2 mM ATPγS, and 10% glycerol).

Channel 3: PBS supplemented with 2 mM Trolox (in the cases of C-DRM1 and C-DRM2) or CMG imaging buffer in the case of CMG.

Channel 4: CMG unwinding buffer (250 mM potassium glutamate, 25 mM HEPES, 10 mM magnesium acetate, 0.02% NP40, 1 mM DTT, 0.1 mg/mL BSA, 2 mM 1,3,5,7 cyclooctatetraene, 2 mM 4-nitrobenzyl alcohol, 2 mM Trolox, 5 mM ATP, and 10% glycerol).

A detailed description of the single-molecule data acquisition will shortly be published by our group (Z.L., E. van Veen, H. Sánchez, B. Solano, F. Palmero Moya, K.A. McCluskey, D.R.M., T. van Laar, and N.H.D., unpublished data). At the beginning of each experiment, the trapping laser power was adjusted to achieve a stiffness of 0.3 pN/nm in both traps (24,46). Then, two beads were trapped in channel 1. Subsequently, individual DNA molecules/DNA:protein complexes were trapped between two beads in channel 2, and we confirmed the tethering of individual DNA molecules by analyzing the force-extension curve (47). The DNA was then transferred to channel 3, the distance between both beads fixed to achieve a tension of 2 pN, and the DNA was illuminated without flow with a 561-nm laser at a power of 7.8 μW (in the case of C-DRM1 and C-DRM2) or 2 μW (in the case of CMG experiments) as measured at the sample plane. Fluorescence signal was detected using a single-photon counting detector. The 2D confocal scans were obtained over an area of 80 $\times$ 20 pixels, which covered the entire DNA and the edges of both beads (Z.L., E. van Veen, H. Sánchez, B. Solano, F. Palmero Moya, K.A. McCluskey, D.R.M., T. van Laar, and N.H.D., unpublished data). Pixel size was set to 50 $\times$ 50 nm, illumination time per pixel was set to 0.2 ms, and the frame rate was set to 600 ms. The microscope outputs HDF5 files storing the confocal scan data, force data, and bead location data monitored during the scan, as well as the force-extension curves. In the case of DNA:CMG complex experiments, the confocal scan sizes were 124 $\times$ 24 pixels and the pixel size was 50 $\times$ 50 nm. Illumination time per pixel was set to 0.2 ms, and the frame rate was set to 10 s.

Data acquisition automation

All single-molecule data were acquired in an automated manner. We used the Lumicks Harbor experiment automation scripts (https://harbor.lumicks.com/scripts) as a starting point (specifically, Joep Vanlier's automation script for trapping beads, trapping DNA, and making force-extension curves) and added the functionality to acquire confocal images after successfully trapping DNA. A detailed description of the automation code steps will shortly be published by our group (Z.L., E. van Veen, H. Sánchez, B. Solano, F. Palmero Moya, K.A. McCluskey, D.R.M., T. van Laar, and N.H.D., unpublished data).

Data analysis

Data analysis software and code

We used Python 3.8 with several libraries for image processing. We used the Laplacian of Gaussian (LoG) detector from Python's "scipy" for spot detection. We used the Linear Assignment Problem method (48) and the "scipy" solver "linear_sum_assignment" to track spots (Z.L., E. van Veen, H. Sánchez, B. Solano, F. Palmero Moya, K.A. McCluskey, D.R.M., T. van Laar, and N.H.D., unpublished data). Bleaching trace analysis was done with the "ruptures" library (Z.L., E. van Veen, H. Sánchez, B. Solano, F. Palmero Moya, K.A. McCluskey, D.R.M., T. van Laar, and N.H.D., unpublished data). The exact Python libraries used and their versions are as follows: numpy = = 1.19.5; matplotlib = = 3.2.2; lumicks-pylake = = 0.7.1; streamlit = = 0.74.1; scipy = = 1.6.1; scikit-image = = 0.16.2; scikit-learn = = 0.23.1; pyyaml = = 5.3.1; pandas = = 1.0.5; pillow = = 7.2.0; tifffile = = 2021.1.11; jupyterlab = = 2.1.5; notebook = = 6.0.3; ruptures = = 1.1.6; pykalman = = 0.9.5.

Overview of data analysis

After acquiring confocal scans, raw image data were processed to generate a table containing the spot detections in each frame. Spot detections are then connected between frames to produce traces that contain location and intensity information over time (Z.L., E. van Veen, H. Sánchez, B. Solano, F. Palmero Moya, K.A. McCluskey, D.R.M., T. van Laar, and N.H.D., unpublished data). A detailed description of the data analysis steps will shortly be published by our group (Z.L., E. van Veen, H. Sánchez, B. Solano, F. Palmero Moya, K.A. McCluskey, D.R.M., T. van Laar, and N.H.D., unpublished data).

Spot detection and tracking

To detect fluorescence spots, we employ the scikit-image implementation of a LoG blob detector (Z.L., E. van Veen, H. Sánchez, B. Solano, F. Palmero Moya, K.A. McCluskey, D.R.M., T. van Laar, and N.H.D., unpublished data) (49). We set the detection radius r_{LoG} to 5 pixels (250 nm); the LoG sigma parameter is given by $\sigma_{LoG} = r_{LoG}/\sqrt{2}$. We set the detection threshold to 0.3 ADU/pixel (for experiments with C-DRM1 and C-DRM2) or 0.5 ADU/pixel (for experiments with C-ZL7 and CMG^{LD555}) (4,8). Spots are then localized with subpixel resolution by fitting a Gaussian profile on spot intensity projections in both x and y directions. To track spots frame by frame, we use our own implementation of the Linear Assignment Problem framework (48) using a maximum spot-linking distance of 6 pixels (300 nm) and a maximum frame gap of three frames (for experiments with C-DRM1 and C-DRM2) or a maximum spot linking distance of 10 pixels (500 nm) and a maximum frame gap of one frame (for experiments with C-ZL7 and CMG^{LD555}).

Determination of number of fluorophores per diffraction-limited spot

To determine the number of fluorophores contained within each diffraction-limited spot, we count the number of photobleaching steps within each spot (Z.L., E. van Veen, H. Sánchez, B. Solano, F. Palmero Moya, K.A. McCluskey, D.R.M., T. van Laar, and N.H.D., unpublished data).

Data filtering

The resulting data tables of traces with number of fluorescent proteins per spot was filtered to reduce noise, outliers, and data that are not suitable for further motion analysis.

1) Diffraction-limited spots containing more than five fluorophores, likely aggregates, are filtered out.
2) Traces starting or ending within 1 kb from the beads are filtered out to exclude fluorophores likely stuck to the beads from entering the dataset.

3) Traces starting after frame 3 (in the case of experiments with C-DRM1 and C-DRM2) or 1 (in the case of experiments with CMG) are also filtered out, as we do not expect any fluorescently labeled molecule to bind the DNA during the scan.

Positional analysis

In all plots that show the positions of diffraction-limited fluorescent spots, we plot the average position of the first three frames of each trace. The bin size of the position histograms was set to 700 bp, a value close to the diffraction limit that takes into account the absolute error in the position coordinate that results from the offset between the brightfield and the confocal channels and the relative error in the position coordinate as measured with a static fluorescent standard (8).

Force-distance analysis

The force-extension curves of individual DNA molecules were fitted in the force range of 5–25 pN using the extensible worm-like chain model (50):

$$\langle x \rangle = L_c \left[1 - \frac{1}{2} \left(\frac{k_B T}{F L_p} \right)^{\frac{1}{2}} + \frac{F}{S} \right] \quad (1)$$

where $\langle x \rangle$ is the end-to-end distance of the DNA, L_p is the persistence length of the DNA, L_c is the contour length of the DNA, S is the stretch modulus of the DNA, k_B is Boltzmann's constant, T is temperature, and F is the pulling force. From the fit, we obtained the parameters L_c, L_p, and S (Figs. 3 *D–G*, *K–N*, and S3 *A–D* in the Supporting Material).

RESULTS

Synthesis of fully custom-sequence 10.1-kb plasmids for single-molecule experiments

To have full control of the sequence of the plasmids used to synthesize DNA constructs for single-molecule experiments, we designed two sets of four custom-sequence 2.5-kb gBlocks. Notably, these gBlocks were designed to contain overlapping sequences of 25–28 bp and a T_m of ∼60°C–63°C at both ends (Fig. 1 *A*). These overlapping end sequences allowed for the unidirectional and scarless assembly of both sets of four gBlocks into two different 10.1-kb plasmids by Gibson Assembly (51) (Fig. 1 *A*, see section "materials and methods"), which we named pDRM1 and pDRM2, respectively. Both these plasmids contain a bacterial origin of replication as well as an ampicillin resistance gene to allow for the bacterial propagation of the newly synthesized plasmids. The assembly reactions were directly transformed into *E. coli*, clones were grown in selection medium, and each plasmid was isolated giving yields of 300–900 ng DNA/mL of bacterial culture (see section "materials and methods"). The most important feature of both custom-sequence plasmids is the number and location of specific restriction enzyme sites that are used to introduce specific features into the single-molecule constructs (Fig. 1 *B* and *D*): pDRM1 contains a unique XhoI restriction site to allow for linearization of the plasmid, five tandem Nb.BbvCI nicking sites separated by 16-bp spacers for the incorporation of one 3′ ssDNA flap, and two BsaI sites separated by 100 bp for the optional cloning of additional DNA sequences into the plasmid via Golden Gate assembly (20) (Fig. 1 *B*). pDRM2 also contains a unique XhoI restriction site to allow for linearization of the plasmid, but it contains two sets of three tandem Nb.BbvCI nicking sites separated by 16-bp spacers for the incorporation of two 3′ ssDNA flaps (1,16,17) (Fig. 1 *D*). To confirm that both sets of gBlocks were assembled scarlessly and in the right order, we sequenced the overlapping regions of the gBlocks as well as the restriction enzyme sites in both plasmids. Furthermore, we carried out test digestions of the plasmids with the restriction enzymes described above and saw either the expected band patterns or bands that can be explained by the incomplete cleavage by some of the enzymes (Fig. 1 *C* and *E*). A full assignment of all the bands can be found in Fig. S1 in the Supporting Material. Taken together, our data show that the two sets of designed gBlocks were successfully and scarlessly assembled in the right order, generating two different 10.1-kb fully custom-sequence plasmids. The whole de novo assembly and plasmid validation procedure takes 3–4 days.

Synthesis of linear 10.1-kb DNA constructs containing an internal ssDNA flap for single-molecule experiments

After confirming the successful assembly of the desired plasmids, we developed a fast (1.5-day long) and efficient method to use these plasmids to synthesize two different 10.1-kb linear DNA constructs containing three biotin moieties at each end for surface attachment and either one (in the case of pDRM1) or two (in the case of pDRM2) internally located ssDNA flaps for helicase binding (see section "materials and methods"; Fig. 2). This method, which we describe step by step in Fig. 2 *A* and *C*, is as follows: we first linearized plasmids pDRM1 and pDRM2 with the restriction enzyme XhoI (Fig. 2 *B*, lanes 1–2; Fig. 2 *D*, lanes 1–2). Digesting the plasmids with XhoI generates 4-nt 5′ overhangs at both ends of the linearized DNA. These overhangs were then biotinylated via a blunting reaction with Klenow fragment DNA polymerase in the presence of biotinylated nucleotides (Fig. 2 *B*, lane 3; Fig. 2 *D*, lane 3), which resulted in the incorporation of three biotin moieties at each end of the DNA. After biotinylation, excess nucleotides were removed by chromatography (see section "materials and methods") and the biotinylated DNA constructs were nicked with the nicking enzyme Nb.BbvCI. After the nicking reaction, we detected some unexpected bands in addition to the expected 10.1-kb band (Fig. 2 *B*, lane 4; Fig. 2 *D*, lane 4). We hypothesized that these additional bands corresponded to products of star endonuclease activity of the nicking enzyme Nb.BbvCI, as their sizes matched what we would expect from full endonuclease activity of Nb.BbvCI: two bands of ∼3.3 and ∼6.8 kb in the case of the construct derived from pDRM1, and three bands of ∼2.5, ∼5.0, and ∼7.5 kb in the case of the construct derived from pDRM2. To test this hypothesis, we digested both biotinylated DNA constructs with full BbvCI endonuclease and

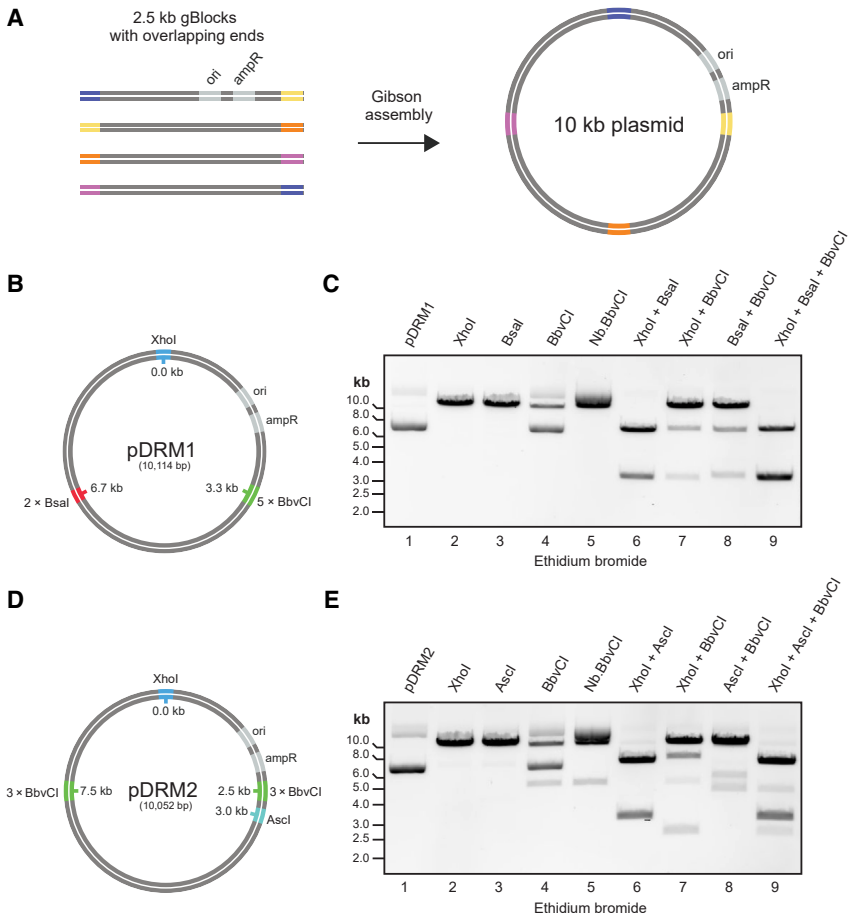

FIGURE 1 Synthesis of fully custom-sequence plasmids from gBlocks. (*A*) Illustration of the plasmid synthesis procedure. Four fully custom-sequence 2.5-kb gBlocks were designed to have pairwise overlapping sequences at their ends (represented in purple, yellow, orange, and pink) to ensure their ordered and scarless assembly into a 10.1-kb plasmid via Gibson Assembly. To ensure bacterial propagation, one of the gBlocks must contain a bacterial origin of replication and an ampicillin resistance gene. (*B*) Diagram of plasmid pDRM1 synthesized as described in (*A*), highlighting the position of restriction enzyme sites to be used for the synthesis of DNA constructs for single-molecule studies. (*C*) Single, double, and triple test restriction digestions of plasmid pDRM1 corroborate the correct order of assembly of the gBlocks used to synthesize it. (*D*) Diagram of plasmid pDRM2 synthesized as described in (*A*), highlighting the position of restriction enzyme sites to be used for the synthesis of DNA constructs for single-molecule studies. (*E*) Single, double, and triple test restriction digestions of plasmid pDRM2 corroborate the correct order of assembly of the gBlocks used to synthesize it. To see this figure in color, go online.

found the same band patterns that we found when we nicked the biotinylated DNA with Nb.BbvCI (Fig. 2 *B*, lanes 4 and 5; Fig. 2 *D*, lanes 4 and 5). After nicking, we heated up the DNA substrates to remove the 16-bp ssDNA spacers between the nicking sites and slowly cooled down the reaction (see section "materials and methods") in the presence of an excess of 3′ Cy3-labeled ssDNA oligos to replace the nicked spacers (11,16,17); these Cy3-labeled oligos are fully complementary to the nicked regions but contain an additional 40-nt 3′ poly-dT to create ssDNA flaps. Of note, to confirm the incorporation of the fluorescent oligos, we scanned the DNA gel with a green laser and saw fluorescent bands at the expected locations (Fig. 2 *B*, lane 6; Fig. 2 *D*, lane 6). After the annealing reaction, we ligated the 5′ end of the fluorescent ssDNA flap(s) overnight with T4 ligase (Fig. 2 *B*, lane 7; Fig. 2 *D*, lane 7), and purified the 10.1-kb bands (Fig. 2 *B*, lane 8; Fig. 2 *D*, lane 8). Finally, in the case of the DNA construct derived from pDRM2 (Fig. 2 *C*), we further confirmed the incorporation of both fluorescent ssDNA flaps by digesting the purified 10.1-kb construct with AscI. The AscI restriction site was engineered to be between the location of both fluorescent forks but off-centered, thus yielding two bands of different sizes (∼3 and ∼7.1 kb). As seen in Fig. 2 *D*, lane 9, both bands contained the fluorescent ssDNA flap, showing that both forks were successfully incorporated into the construct derived from pDRM2. After the final purification, we consistently had yields of ∼10%–15% relative to the initial amount of plasmid DNA, which are significantly higher than typical multi-ligation-based protocols. We henceforth call the synthesized constructs C-DRM1 and C-DRM2, respectively.

Single-molecule characterization of DNA C-DRM1 and C-DRM2

We then proceeded to characterize both synthesized DNA constructs at the single-molecule level. For this, we used a combination of dual optical trapping and confocal scanning microscopy (43) to monitor the presence of fluorescent ssDNA flap diffraction-limited spots on single DNA molecules held in an optical trap (Fig. 3 *A* and *H*; see section "materials and methods"). First, we monitored the efficiency of fluorescent ssDNA flap incorporation by counting the number of fluorescent spots in each DNA molecule. We found that, in the case of C-DRM1, ∼82% of the trapped DNA molecules contained one fluorescent spot (Fig. 3 *B*) and, in the case of construct C-DRM2, ∼79% of the trapped DNA molecules contained two fluorescent spots (Fig. 3 *I*). These fork

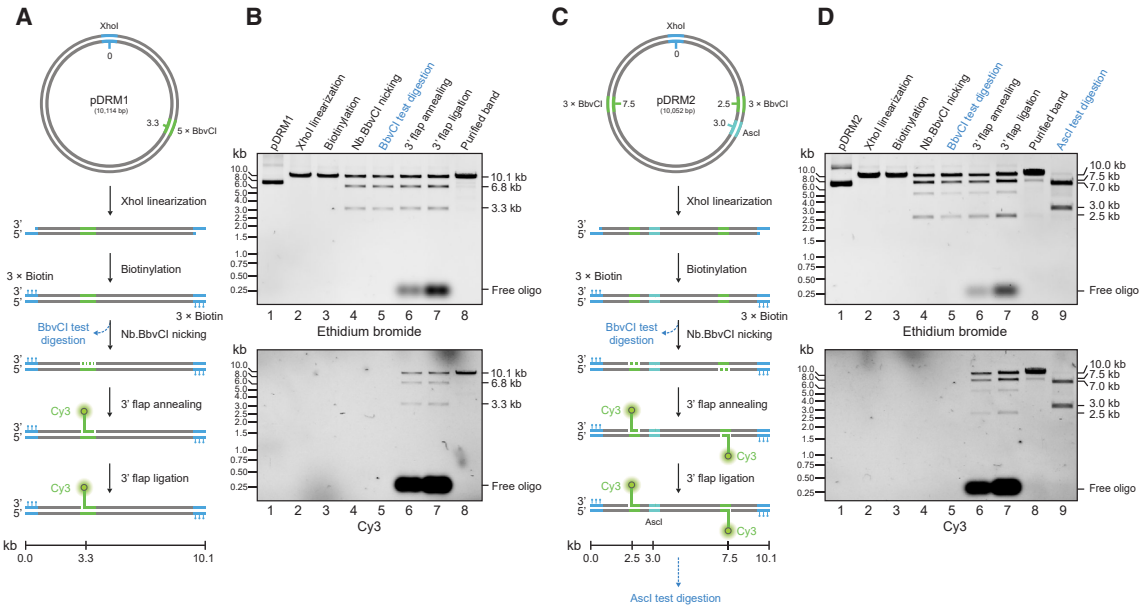

FIGURE 2 Synthesis of 10.1-kb linear DNA constructs with biotinylated ends and internal 3' flaps for single-molecule experiments. (*A*) Step-by-step pictorial description of the synthesis of construct C-DRM1 using pDRM1 as a starting substrate. (*B*) Agarose gel monitoring of each of the steps described in (*A*) showing either total DNA stained with ethidium bromide (*top*) or Cy3-labeled DNA illuminated with a green laser (*bottom*). (*C*) Step-by-step pictorial description of the synthesis of construct C-DRM2 using pDRM2 as a starting substrate. (*D*) Agarose gel monitoring of each of the steps described in (*C*) showing either total DNA stained with ethidium bromide (*top*) or Cy3-labeled DNA illuminated with a green laser (*bottom*). Steps colored in blue are control test restriction digestions that are not part of the synthesis procedure. To see this figure in color, go online.

incorporation efficiencies likely reflect the actual ssDNA flap incorporation efficiency, as our measured labeling efficiencies of the flap oligos were ∼100% (see section "materials and methods"). Of note, we counted the number of photobleaching steps within each diffraction-limited spot and found that all the detected spots photobleached in one step (Fig. S2 *A* and *B* in the Supporting Material), confirming that we incorporated one ssDNA flap at each nicking location (Fig. 2 *A* and *C*). We next proceeded to analyze the position of the fluorescent ssDNA flaps along the DNA. Notably, as we cannot differentiate between the two possible orientations that the DNA can have in the optical tweezers, we display the position of the fluorescent spots as distances from the DNA center (4,8). This analysis confirmed that the forks were incorporated at the expected locations on the DNA (Fig. 3 *C* and *J*). We also obtained force-extension curves for both DNA constructs (47) and fitted the obtained curves with an extensible worm-like chain model (50) (Fig. 3 *D* and *K*). From this model, we obtained three parameters: contour length, persistence length, and stretch modulus (50). The average contour lengths obtained for both constructs agreed with the expected values within experimental error (Fig. 3 *E* and *L*), and the average persistence length and stretch modulus for each of the two DNA constructs in the buffer conditions employed agreed with previously reported values (52,53) (Fig. 3 *F*, *G*, *M*, and *N*). This single-molecule characterization confirmed that we synthesized the expected DNA constructs in an efficient manner.

Demonstration of ssDNA flap binding and unwinding by a helicase

Having validated the DNA synthesis method, we sought to assess whether the incorporated 3′ ssDNA flap can be bound by the 3′-to-5′ eukaryotic replicative helicase CMG (10,13,29,54) and whether the helicase could then translocate in the expected direction. To this end, we used pDRM1 as a template and cloned into it a ∼6.5-kb duplex region (Fig. 1 *B*; see section "materials and methods"), yielding a longer version of plasmid pDRM1 that we named pZL7. Following the same method described above, we used plasmid pZL7 to synthesize DNA construct C-ZL7 (Fig. 4 *A*). Of note, to prevent any artifacts caused by the presence of a 3′ fluorophore in the binding site of the helicase, C-ZL7 contains a non-fluorescently labeled ssDNA flap. We first characterized C-ZL7 by force spectroscopy (47,50) (Fig. S3 *A*) in the same way that we did for C-DRM1 and C-DRM2, and obtained an average value for the contour length that agreed with the expected value within experimental error (Fig. S3 *B*), and average persistence length and stretch modulus values (Fig. S3 *C* and *D*) that agree with previously reported values in the buffer conditions employed (52,53). We then incubated construct C-ZL7 with fluorescently labeled $CMG^{Cdc45\text{-}LD555}$. We first incubated $CMG^{Cdc45\text{-}LD555}$ with C-ZL7 in bulk in the presence of the slowly hydrolyzable ATP analog ATPγS to allow $CMG^{Cdc45\text{-}LD555}$ to bind to the 3′ ssDNA flap in C-ZL7

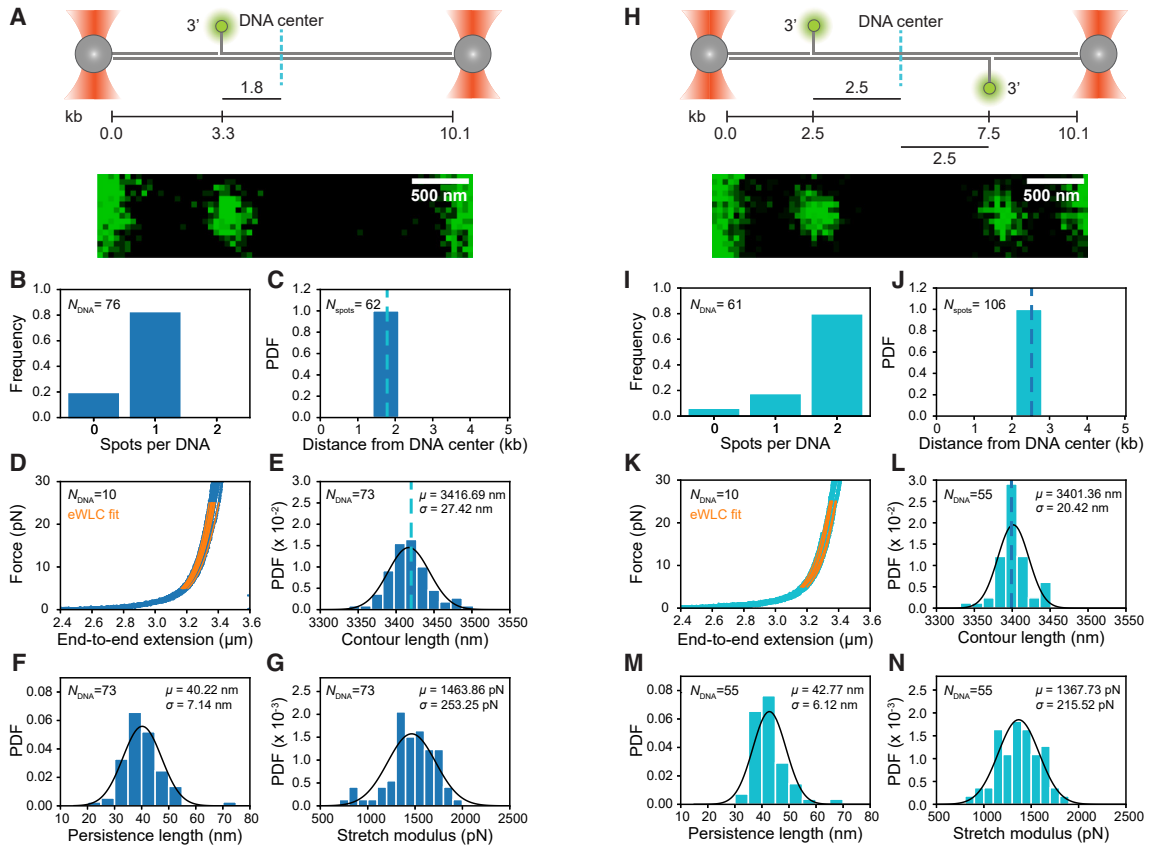

FIGURE 3 Single-molecule characterization of DNA constructs C-DRM1 and C-DRM2. (*A*) Diagram of construct C-DRM1 (*top*) together with an example confocal scan of a C-DRM1 molecule held in place in an optical trap (*bottom*). (*B*) Distribution of numbers of Cy3 diffraction-limited spots per molecule of construct C-DRM1. (*C*) Probability density function of positions from the DNA center of Cy3 diffraction-limited spots in C-DRM1. Dotted cyan line indicates the expected position from the DNA center of the fluorescent ssDNA flap. (*D*) Example force-extension curves of construct C-DRM1 (*blue*) together with the fitted extensible worm-like chain (eWLC) model plotted in the force range used for fitting (orange). (*E–G*) Probability density function of contour lengths (*E*), persistence lengths (*F*), and stretch moduli (*G*) obtained from the eWLC model fits of force-extension curves of C-DRM1; black lines show a Gaussian fit of the data, and μ and σ are the mean and the standard deviation of the data, respectively. Dotted cyan line in (*E*) shows the expected contour length of C-DRM1. (*H*) Diagram of construct C-DRM2 (*top*) together with an example confocal scan of a C-DRM2 molecule held in place in an optical trap (*bottom*). (*I*) Distribution of numbers of Cy3 diffraction-limited spots per molecule of construct C-DRM2. (*J*) Probability density function of positions from the DNA center of Cy3 diffraction-limited spots in C-DRM2. Dotted blue line indicates the expected position from the DNA center of the fluorescent ssDNA flaps. (*K*) Example force-extension curves of construct C-DRM2 (*cyan*) together with the fitted eWLC model plotted in the force range used for fitting (*orange*). (*L–N*) Probability density function of contour lengths (*L*), persistence lengths (*M*), and stretch moduli (*N*) obtained from the eWLC model fits of force-extension curves of C-DRM2; black lines show a Gaussian fit of the data, and μ and σ are the mean and the standard deviation of the data, respectively. Dotted blue line in (*L*) shows the expected contour length of C-DRM2. To see this figure in color, go online.

without unwinding it (12,29) (see section "materials and methods"). We then diluted the reaction and flowed it into our optical tweezers. Notably, our optical tweezers are equipped with a microfluidic flow cell that allows us to buffer exchange the trapped DNA:protein complex in situ (4,8,43). Using this flow cell, we moved the trapped DNA:CMG$^{Cdc45\text{-}LD555}$ complexes into buffer solution containing ATP and immediately started to image CMG motion. We found that 78.3% of the trapped DNA contained CMG$^{Cdc45\text{-}LD555}$ diffraction-limited spots (Fig. 4 *B*), which is consistent with our measured ssDNA flap incorporation efficiency in pDRM1 (Fig. 3 *B*). Of these spots, 74.5% contained one CMG complex (Fig. 4 *C*). As can be seen in Fig. 4 *D*, the vast majority of the CMG spots were initially located at the expected position of the ssDNA flap. Furthermore, as seen in Fig. 4 *D* and *E*, we detected motion of CMG$^{Cdc45\text{-}LD555}$ that started at the expected 3′ ssDNA flap location and proceeded in the expected 3′-to-5′ direction, thereby showing that our method to synthesize DNA constructs results in a 3′ ssDNA flap that can be bound and translocated from by a helicase. The observed long-range translocation also shows that the ssDNA flap is successfully ligated, as CMG has been previously reported to dissociate from DNA at nicks (30).

DISCUSSION

We describe a method to synthesize fully custom-sequence DNA constructs for single-molecule studies. For this, we use Gibson Assembly (51) to assemble fully custom-sequence

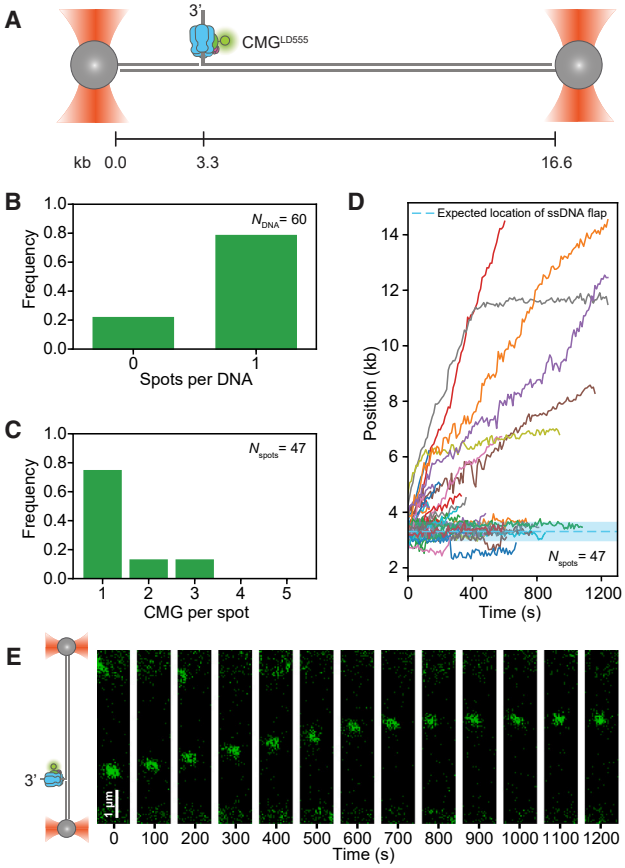

FIGURE 4 Functional validation of the introduced 3′ ssDNA flaps. (*A*) Diagram of construct C-ZL7 held in place in an optical trap and containing a fluorescently labeled CMG helicase bound to the 3′ ssDNA flap. (*B*) Distribution of numbers of fluorescently labeled CMG diffraction-limited spots per molecule of construct C-ZL1. (*C*) Distribution of numbers of fluorescently labeled CMG complexes within each diffraction-limited spot. (*D*) Position along DNA construct C-ZL1 versus time of fluorescently labeled CMG spots. For clarity, the traces have been compensated for DNA orientation; i.e., they have been rotated so that the initial positions of all traces are within the same half of the DNA. Note that this rotation does not automatically place the start of the trace at the expected location of the ssDNA flap. (*E*) Example kymograph of a fluorescently labeled CMG helicase initially bound at the expected location of the ssDNA flap, which translocates unidirectionally in a 3′-to-5′ direction upon the addition of ATP. To see this figure in color, go online.

gBlocks into two different 10.1-kb plasmids (Fig. 1) using a simple and fast *in vitro* protocol that takes 3–4 days. This approach allowed us to generate large amounts of plasmid by propagation in standard *E. coli* strains (see section "materials and methods"). In this work, we assembled two plasmids of 10.1 kb in length, as this length sufficed for the downstream production of linear DNA molecules suited to single-molecule experiments. However, Gibson Assembly has also been used to efficiently clone genomic fragments of up to 100 kb in length into plasmids using overlapping sequences of similar lengths to the ones used in this study (55), suggesting that the de novo synthesis of much larger plasmids may be easily achievable. Further studies to determine the length limit in these assembly reactions will be of interest. The use of Gibson Assembly to assemble fully custom-sequence plasmids from gBlocks alone, as done in this study, provides a novel methodology in the field of single-molecule biophysics. We believe that the protocol of plasmid assembly we describe will allow other scientists working on a wide variety of DNA-processing mechanisms to design more biologically relevant DNA constructs as well as to investigate the role of DNA sequence on many of these processes with unprecedented control.

Using our de novo assembled plasmids, we developed a fast (1.5-day long) and efficient approach to synthesize two different linear constructs containing end and internal modifications for single-molecule force and fluorescence spectroscopy experiments (Fig. 2). As a proof of principle, we incorporated either one or two internal ssDNA flaps into our constructs and characterized them in bulk (Fig. 2) and at the single-molecule level (Fig. 3). Finally, we functionally validated our approach at the single-molecule level by showing that the incorporated ssDNA flaps can be bound by the eukaryotic replicative helicase CMG, which then translocates in the expected direction (Fig. 4). Notably, the CMG that we employed in this study has been previously studied in correlative optical tweezers and fluorescence experiments after loading it onto λ phage DNA in a nonspecific manner after generating ssDNA regions in the otherwise double-stranded DNA (dsDNA) construct by the use of high force (24); this approach does not only lack control of the loading site of the helicase but also lacks control of the number of helicases that can be loaded at the long stretches of ssDNA generated, and could also have force-related artifacts. The new approach that we developed in this study will not only allow us and others to site-specifically bind CMG to the DNA without the use of high force but also allow us and others to study the motion of CMG along a DNA substrate with a fully controlled sequence.

Although in this proof of concept study we introduced 3′ ssDNA flaps, the directionality of the ssDNA flaps can easily be reversed without modifying the DNA sequence through the use of the complementary nicking enzyme to the one used in this study (16,17). Additionally, we expect/anticipate that the same protocol can be used to easily incorporate other DNA modifications relevant to the study of DNA repair and DNA secondary structure processing, such as ssDNA/dsDNA junctions, hairpins, and G-quadruplexes (16,18,56–58). Furthermore, our synthesis strategy can easily be used to incorporate noncanonical nucleotides in the form of modified oligos (1,16,17), allowing for the introduction of a wide range of chemical moieties that in turn facilitate the site-specific covalent and noncovalent attachment of other molecules of interest (e.g., protein crosslinks, streptavidin, fluorophores) (1,12,14,16,17,59) to the DNA, all within a fully controlled sequence context. Finally, even without the introduction of extrahelical/noncanonical structures, we anticipate that our method will benefit the field by allowing full control of

the sequence background used to study a wide range of DNA:protein interactions.

DATA AND CODE AVAILABILITY

Raw and processed ensemble and single-molecule data supporting the findings of this study have been deposited in the 4TU.ResearchData repository and can be found at https://doi.org/10.4121/fe506b56-0ae0-4b89-9a5d-654b8b222cb0. The repository contains a table with an overview of experiments; force-distance tables sorted by experimental condition; spot position and intensity tables sorted by experimental condition; filtered spot tracking tables, with connected spot detections for each frame in each scan, each row having a scan_id and trace_id; and example TIFF files. All the code used in the current study is available at https://gitlab.tudelft.nl/nynke-dekker-lab/public/flapped-DNA-synthesis.

SUPPORTING MATERIAL

Supporting material can be found online at https://doi.org/10.1016/j.bpj.2023.11.008.

AUTHOR CONTRIBUTIONS

D.R.M. conceived the study, and N.D. supervised it. D.R.M. designed, assembled, and characterized plasmids pDRM1 and pDRM2. D.R.M. developed the synthesis strategy for the single-molecule constructs used in this study and synthesized constructs C-DRM1 and C-DRM2. Z.L. assembled and characterized plasmid pZL7 and synthesized construct C-ZL7. D.R.M. conducted the single-molecule experiments with DNA constructs C-DRM1 and C-DRM2 with input from Z.L. Z.L. expressed, purified, and fluorescently labeled CMG and conducted the single-molecule experiments with C-ZL7 and CMG. Z.L. wrote automation and force spectroscopy analysis scripts. D.R.M. analyzed the data. All authors were involved in the discussion of the data. D.R.M. wrote the manuscript with input from Z.L. and N.D.

ACKNOWLEDGMENTS

We thank N.D. lab members Theo van Laar, Julien Gros, Katinka Ligthart, Nerea Murugarren, Pang Yen Wang, and Humberto Sánchez, as well as Miloš Cvetković, Alessandro Costa, Samson Glaser, and John Diffley for their help with the expression, purification, and labeling of CMG. We also thank Vincent Kruit and Elena Radul for their help with the initial characterization of plasmid pDRM2 and the assembly of plasmid pZL7.

Funding: DRM acknowledges funding from a Boehringer Ingelheim Fonds PhD fellowship. Z.L. acknowledges funding from an EMBO Postdoctoral Fellowship (ALTF 484-2022). N.D. acknowledges funding from the Netherlands Organisation for Scientific Research (NWO) through TOP grant 714.017.002, from the BaSyC—Building a Synthetic Cell Gravitation grant (024.003.019) of the Netherlands Ministry of Education, Culture and Science (OCW), and from the European Research Council through an Advanced Grant (REPLICHROMA; grant number 789267).

DECLARATION OF INTERESTS

The authors declare no competing interests.

REFERENCES

1. Yardimci, H., X. Wang, …, J. C. Walter. 2012. Bypass of a protein barrier by a replicative DNA helicase. *Nature.* 492:205–209.
2. Ticau, S., L. J. Friedman, …, S. P. Bell. 2015. Single-molecule studies of origin licensing reveal mechanisms ensuring bidirectional helicase loading. *Cell.* 161:513–525.
3. Ticau, S., L. J. Friedman, …, S. P. Bell. 2017. Mechanism and timing of Mcm2-7 ring closure during DNA replication origin licensing. *Nat. Struct. Mol. Biol.* 24:309–315.
4. Sánchez, H., K. McCluskey, …, N. H. Dekker. 2021. DNA replication origins retain mobile licensing proteins. *Nat. Commun.* 12:1908.
5. Scherr, M. J., S. A. Wahab, …, K. E. Duderstadt. 2022. Mobile origin-licensing factors confer resistance to conflicts with RNA polymerase ll ll Mobile origin-licensing factors confer resistance to conflicts with RNA polymerase. *Cell Rep.* 38, 110531.
6. Díaz-Celis, C., C. Cañari-Chumpitaz, …, C. Bustamante. 2022. Assignment of structural transitions during mechanical unwrapping of nucleosomes and their disassembly products. *Proc. Natl. Acad. Sci. USA.* 119:1–11.
7. Safaric, B., E. Chacin, …, K. E. Duderstadt. 2022. The fork protection complex recruits FACT to reorganize nucleosomes during replication. *Nucleic Acids Res.* 50:1317–1334.
8. Ramírez Montero, D., H. Sánchez, …, N. H. Dekker. 2023. Nucleotide binding halts diffusion of the eukaryotic replicative helicase during activation. *Nat. Commun.* 14:2082.
9. Zhang, B., W. Q. Wu, …, X. G. Xi. 2016. G-quadruplex and G-rich sequence stimulate Pif1p-catalyzed downstream duplex DNA unwinding through reducing waiting time at ss/dsDNA junction. *Nucleic Acids Res.* 44:8385–8394.
10. Lewis, J. S., L. M. Spenkelink, …, A. M. Van Oijen. 2017. Single-molecule visualization of Saccharomyces cerevisiae leading-strand synthesis reveals dynamic interaction between MTC and the replisome. *Proc. Natl. Acad. Sci. USA.* 114:10630–10635.
11. Kim, Y., A. De La Torre, I. J. Finkelstein…, 2017. Efficient modification of λ-DNA substrates for single-molecule studies. *Sci. Rep.* 7:2071.
12. Kose, H. B., N. B. Larsen, …, H. Yardimci. 2019. Dynamics of the Eukaryotic Replicative Helicase at Lagging-Strand Protein Barriers Support the Steric Exclusion Model. *Cell Rep.* 26:2113–2125.e6.
13. Lewis, J. S., L. M. Spenkelink, …, A. M. van Oijen. 2020. Tunability of DNA polymerase stability during eukaryotic DNA replication. *Mol. Cell.* 77:17–25.e5.
14. Sparks, J. L., G. Chistol, …, J. C. Walter. 2019. The CMG Helicase Bypasses DNA-Protein Cross-Links to Facilitate Their Repair. *Cell.* 176:167–181.e21.
15. Kaczmarczyk, A. P., A. C. Déclais, …, D. S. Rueda. 2022. Search and Processing of Holliday Junctions within Long DNA by Junction-Resolving Enzymes. *Nat. Commun.* 13:5921.
16. Luzzietti, N., H. Brutzer, …, R. Seidel. 2011. Efficient preparation of internally modified single-molecule constructs using nicking enzymes. *Nucleic Acids Res.* 39:e15.
17. Luzzietti, N., S. Knappe, …, R. Seidel. 2012. Nicking enzyme-based internal labeling of DNA at multiple loci. *Nat. Protoc.* 7:643–653.
18. Belan, O., C. Barroso, …, S. J. Boulton. 2021. Article Single-molecule analysis reveals cooperative stimulation of Rad51 filament nucleation and growth by mediator proteins Article Single-molecule analysis reveals cooperative stimulation of Rad51 filament nucleation and growth by mediator proteins. *Mol. Cell.* 81:1–16.
19. Mueller, S. H., L. M. Spenkelink, …, J. S. Lewis. 2020. Design of customizable long linear DNA substrates with controlled end modifications for single-molecule studies. *Anal. Biochem.* 592, 113541.
20. Bell, N. A. W., and J. E. Molloy. 2022. Efficient golden gate assembly of DNA constructs for single molecule force spectroscopy and imaging. *Nucleic Acids Res.* 50:E77.
21. Pradhan, B., T. Kanno, …, E. Kim. 2023. The Smc5/6 complex is a DNA loop-extruding motor. *Nature.* 616:843–848.

22. Wang, F., S. Redding, …, E. C. Greene. 2013. The promoter-search mechanism of Escherichia coli RNA polymerase is dominated by three-dimensional diffusion. *Nat. Struct. Mol. Biol.* 20:174–181.

23. Ganji, M., I. A. Shaltiel, …, C. Dekker. 2018. Real-time imaging of DNA loop extrusion by condensin. *Science.* 360:102–105.

24. Wasserman, M. R., G. D. Schauer, …, S. Liu. 2019. Replication Fork Activation Is Enabled by a Single-Stranded DNA Gate in CMG Helicase. *Cell.* 178:600–611.e16.

25. Kapadia, N., Z. W. El-Hajj, …, R. Reyes-Lamothe. 2020. Processive Activity of Replicative DNA Polymerases in the Replisome of Live Eukaryotic Cells. *Mol. Cell.* 80:114–126.e8.

26. Lee, C. Y., and S. Myong. 2021. Probing steps in DNA transcription using single-molecule methods. *J. Biol. Chem.* 297, 101086.

27. Tanasie, N. L., P. Gutiérrez-Escribano, …, J. Stigler. 2022. Stabilization of DNA fork junctions by Smc5/6 complexes revealed by single-molecule imaging. *Cell Rep.* 41:111778.

28. Silverstein, T. D., B. Gibb, and E. C. Greene. 2014. Visualizing protein movement on DNA at the single-molecule level using DNA curtains. *DNA Repair.* 20:94–109.

29. Kose, H. B., S. Xie, …, H. Yardimci. 2020. Duplex DNA engagement and RPA oppositely regulate the DNA-unwinding rate of CMG helicase. *Nat. Commun.* 11:3713–3715.

30. Vrtis, K. B., J. M. Dewar, …, J. C. Walter. 2021. Single-strand DNA breaks cause replisome disassembly. *Mol. Cell.* 81:1309–1318.e6.

31. Newton, M. D., B. J. Taylor, …, D. S. Rueda. 2019. DNA stretching induces Cas9 off-target activity. *Nat. Struct. Mol. Biol.* 26:185–192.

32. Low, E., G. Chistol, …, J. C. Walter. 2020. The DNA replication fork suppresses CMG unloading from chromatin before termination. *Genes Dev.* 34:1534–1545.

33. Gruszka, D. T., S. Xie, …, H. Yardimci. 2020. Single-molecule imaging reveals control of parental histone recycling by free histones during DNA replication. *Sci. Adv.* 6, eabc0330.

34. Thorpe, H. M., and M. C. Smith. 1998. In vitro site-specific integration of bacteriophage DNA catalyzed by a recombinase of the-resolvase/invertase family. *Proc. Natl. Acad. Sci. USA.* 95:5505–5510.

35. Thomason, L. C., A. B. Oppenheim, and D. L. Court. 2009. Modifying Bacteriophage λ with Recombineering. *Methods Mol. Biol.* 501:239–251.

36. Bell, J. C., J. L. Plank, …, S. C. Kowalczykowski. 2012. Direct imaging of RecA nucleation and growth on single molecules of SSB-coated ssDNA. *Nature.* 491:274–278.

37. Burnham, D. R., H. B. Kose, H. Yardimci…, 2019. The mechanism of DNA unwinding by the eukaryotic replicative helicase. *Nat. Commun.* 10:2159.

38. Naegeli, H., L. Bardwell, and E. C. Friedberg. 1993. Inhibition of Rad3 DNA Helicase Activity by DNA Adducts and Abasic Sites: Implications for the Role of a DNA Helicase in Damage-Specific Incision of DNA. *Biochemistry.* 32:613–621.

39. von Hippel, P. H., and A. H. Marcus. 2019. The many roles of binding cooperativity in the control of DNA replication. *Biophys. J.* 117:2043–2046.

40. Van Loenhout, M. T. J., M. V. De Grunt, and C. Dekker. 2012. Dynamics of DNA supercoils. *Science.* 338:94–97.

41. Whinn, K. S., G. Kaur, …, H. Ghodke. 2019. Nuclease dead Cas9 is a programmable roadblock for DNA replication. *Sci. Rep.* 9:13292–13299.

42. Schauer, G. D., L. M. Spenkelink, …, M. E. O'Donnell. 2020. Replisome bypass of a protein-based R-loop block by Pif1. *Proc. Natl. Acad. Sci. USA.* 117:30354–30361.

43. Candelli, A., G. J. L. Wuite, and E. J. G. Peterman. 2011. Combining optical trapping, fluorescence microscopy and micro-fluidics for single molecule studies of DNA-protein interactions. *Phys. Chem. Chem. Phys.* 13:7263–7272.

44. Dijk, M. A. v., L. C. Kapitein, …, E. J. G. Peterman. 2004. Combining optical trapping and single-molecule fluorescence spectroscopy: Enhanced photobleaching of fluorophores. *J. Phys. Chem. B.* 108:6479–6484.

45. Spakman, D., G. A. King, …, G. J. L. Wuite. 2020. Constructing arrays of nucleosome positioning sequences using Gibson Assembly for single-molecule studies. *Sci. Rep.* 10:9903–9911.

46. Candelli, A., J. T. Holthausen, …, E. J. G. Peterman. 2014. Visualization and quantification of nascent RAD51 filament formation at single-monomer resolution. *Proc. Natl. Acad. Sci. USA.* 111:15090–15095.

47. Bustamante, C., J. F. Marko, …, S. Smith. 1994. Entropic Elasticity of lambda-Phage DNA. *Science.* 265:1599–1600.

48. Jaqaman, K., D. Loerke, …, G. Danuser. 2008. Robust single-particle tracking in live-cell time-lapse sequences. *Nat. Methods.* 5:695–702.

49. Van Der Walt, S., J. L. Schönberger, …, T. Yu. 2014. Scikit-image: Image processing in python. *PeerJ.* 1–18.

50. Odijk, T. 1995. Stiff Chains and Filaments under Tension. *Macromolecules.* 28:7016–7018.

51. Gibson, D. G., L. Young, …, H. O. Smith. 2009. Enzymatic assembly of DNA molecules up to several hundred kilobases. *Nat. Methods.* 6:343–345.

52. Wang, M. D., H. Yin, …, S. M. Block. 1997. Stretching DNA with optical tweezers. *Biophys. J.* 72:1335–1346.

53. Baumann, C. G., S. B. Smith, …, C. Bustamante. 1997. Ionic effects on the elasticity of single DNA molecules. *Proc. Natl. Acad. Sci. USA.* 94:6185–6190.

54. Moyer, S. E., P. W. Lewis, and M. R. Botchan. 2006. Isolation of the Cdc45/Mcm2-7/GINS (CMG) complex, a candidate for the eukaryotic DNA replication fork helicase. *Proc. Natl. Acad. Sci. USA.* 103:10236–10241.

55. Jiang, W., X. Zhao, …, T. F. Zhu. 2015. Cas9-Assisted Targeting of CHromosome segments CATCH enables one-step targeted cloning of large gene clusters. *Nat. Commun.* 6:8101–8108.

56. Dhakal, S., Y. Cui, …, H. Mao. 2013. Structural and mechanical properties of individual human telomeric G-quadruplexes in molecularly crowded solutions. *Nucleic Acids Res.* 41:3915–3923.

57. Parks, J. W., and M. D. Stone. 2017. Single-Molecule Studies of Telomeres and Telomerase. *Annu. Rev. Biophys.* 46:357–377.

58. Belan, O., G. Moore, …, D. S. Rueda. 2021. Generation of versatile ss-dsDNA hybrid substrates for single-molecule analysis. *STAR Protoc.* 2, 100588.

59. Duxin, J. P., J. M. Dewar, …, J. C. Walter. 2014. Repair of a DNA-protein crosslink by replication-coupled proteolysis. *Cell.* 159:346–357.